Research Article | Vol. 26, No. 10 | 14 May 2018 | OPTICS EXPRESS 13461
Optics EXPRESS

Real-time compensation of errors in refractive index shift measurements of microring sensors using thermo-optic coefficients

PRASHANTH R. PRASAD,[1,2] SHANKAR K. SELVARAJA,[1] AND MANOJ VARMA[1,2]

[1] *Centre for Nano Science and Engineering, Indian Institute of Science, Bangalore-560012, India*
[2] *Department of Electrical Communication Engineering, Indian Institute of Science, Bangalore-560012, India*
[*] *mvarma@iisc.ac.in*

Abstract: We report a method for compensation of errors caused by temperature fluctuations in refractive index measurements using Silicon photonic microring sensors. The method involves determination of resonance wavelength shifts caused by thermal fluctuations using real-time measurement of on-chip temperature variations and thermo-optic coefficient (TOC) of analyte liquids. Resistive metal lines patterned around Silicon microrings are used to track temperature variations and TOC of analyte is calculated by measuring wavelength shifts caused by controlled increments in device temperature. The TOC of de-ionized water is determined to be $-1.12 \times 10^{-4}/°C$, with an accuracy of $\pm 8.26 \times 10^{-6}/°C$. In our system, chip-surface temperature variations were measured with an instrument limited precision of 0.004 °C yielding a factor of 16 enhancement in tracking accuracy compared to conventional, bottom-of-chip temperature measurement. We show that refractive index detection limit of the microring sensor is also improved by the same factor.

OCIS codes: (130.0130) Integrated optics; (130.6010) Sensors; (230.5750) Resonators.

References and links

1. M. Estevez, M. Alvarez, and L. Lechuga, "Integrated optical devices for lab-on-a-chip biosensing applications," Laser Photonics Rev. **6**, 463–487 (2012).
2. D. X. Xu, A. Densmore, A. Delâge, P. Waldron, R. McKinnon, S. Janz, J. Lapointe, G. Lopinski, T. Mischki, E. Post, P. Cheben, and J. H. Schmid, "Folded cavity SOI microring sensors for high sensitivity and real time measurement of biomolecular binding," Opt. Express **16**, 15137–15148 (2008).
3. J. Niehusmann, A. Vörckel, P. H. Bolivar, T. Wahlbrink, W. Henschel, and H. Kurz, "Ultrahigh-quality-factor silicon-on-insulator microring resonator," Opt. Lett. **29**, 2861–2863 (2004).
4. K. De Vos, I. Bartolozzi, E. Schacht, P. Bienstman, and R. Baets, "Silicon-on-Insulator microring resonator for sensitive and label-free biosensing," Opt. Express **15**, 7610–7615 (2007).
5. K. De Vos, J. Girones, T. Claes, Y. De Koninck, S. Popelka, E. Schacht, R. Baets, and P. Bienstman, "Multiplexed Antibody Detection With an Array of Silicon-on-Insulator Microring Resonators," IEEE Photon. J. **1**, 225–235 (2009).
6. M. Iqbal, M. A. Gleeson, B. Spaugh, F. Tybor, W. G. Gunn, M. Hochberg, T. Baehr-Jones, R. C. Bailey, and L. C. Gunn, "Label-Free Biosensor Arrays Based on Silicon Ring Resonators and High-Speed Optical Scanning Instrumentation," IEEE J. Sel. Topics Quantum Electron. **16**, 654–661 (2010).
7. J. Koo and C. Kleinstreuer, "Viscous dissipation effects in microtubes and microchannels," Int. J. Heat Mass Transfer **47**, 3159 – 3169 (2004).
8. B. J. Frey, D. B. Leviton, and T. J. Madison, "Temperature-dependent refractive index of silicon and germanium," Proc. SPIE 6273, 62732J (2006).
9. W. Bogaerts, M. Fiers, and P. Dumon, "Design Challenges in Silicon Photonics," IEEE J. Sel. Topics Quantum Electron. **20**, 1–8 (2014).
10. D.-X. Xu, M. Vachon, A. Densmore, R. Ma, S. Janz, A. Delâge, J. Lapointe, P. Cheben, J. H. Schmid, E. Post, S. Messaoudène, and J.-M. Fédéli, "Real-time cancellation of temperature induced resonance shifts in SOI wire waveguide ring resonator label-free biosensor arrays," Opt. Express **18**, 22867–22879 (2010).
11. L. Stern, A. Naiman, G. Keinan, N. Mazurski, M. Grajower, and U. Levy, "Ultra-precise optical to radio frequency based chip-scale refractive index and temperature sensor," Optica **4**, 1–7 (2017).

#320805 https://doi.org/10.1364/OE.26.013461
Journal © 2018 Received 26 Jan 2018; revised 28 Feb 2018; accepted 7 Mar 2018; published 10 May 2018

Optics EXPRESS

12. V. Raghunathan, W. N. Ye, J. Hu, T. Izuhara, J. Michel, and L. Kimerling, "Athermal operation of Silicon waveguides: spectral, second order and footprint dependencies," Opt. Express **18**, 17631–17639 (2010).
13. J. T. Robinson, K. Preston, O. Painter, and M. Lipson, "First-principle derivation of gain in high-index-contrast waveguides,"Opt. Express **16**, 16659–16669 (2008).
14. P. E. Ciddor, "Refractive index of air: new equations for the visible and near infrared," Appl. Opt. **35**, 1566–1573 (1996).
15. D. B. Leviton and B. J. Frey, "Temperature-dependent absolute refractive index measurements of synthetic fused silica," arXiv:0805.0091 (2008).
16. J. E. Saunders, C. Sanders, H. Chen, and H.-P. Loock, "Refractive indices of common solvents and solutions at 1550 nm," Appl. Opt. **55**, 947–953 (2016).
17. C. V. Rumens, M. A. Ziai, K. E. Belsey, J. C. Batchelor, and S. J. Holder, "Swelling of pdms networks in solvent vapours; applications for passive rfid wireless sensors," J. Mater. Chem. C **3**, 10091–10098 (2015).
18. C.-L. Lee, H.-Y. Ho, J.-H. Gu, T.-Y. Yeh, and C.-H. Tseng, "Dual hollow core fiber-based Fabry-Perot interferometer for measuring the thermo-optic coefficients of liquids," Opt. Lett. **40**, 459–462 (2015).
19. Y. H. Kim, S. J. Park, S.-W. Jeon, S. Ju, C.-S. Park, W.-T. Han, and B. H. Lee, "Thermo-optic coefficient measurement of liquids based on simultaneous temperature and refractive index sensing capability of a two-mode fiber interferometric probe,"Opt. Express **20**, 23744–23754 (2012).
20. C.-B. Kim and C. B. Su, "Measurement of the refractive index of liquids at 1.3 and 1.5 micron using a fibre optic Fresnel ratio meter," Meas. Sci. Technol.**15**, 1683–1686 (2004).
21. S.-J. Qiu, Y. Chen, F. Xu, and Y.-Q. Lu, "Temperature sensor based on an isopropanol-sealed photonic crystal fiber in-line interferometer with enhanced refractive index sensitivity," Opt. Lett. **37**, 863–865 (2012).

1. Introduction

Silicon photonic sensors have been studied extensively for measurement of refractive index shift in liquids. Their unique advantages such as small size and the potential for large-scale manufacture using CMOS compatible technologies have made them promising candidates for applications in several areas including healthcare, biomedical research and environmental monitoring [1]. Among various implementations of Silicon photonic sensors, microring resonators have been investigated widely because of their compactness [2], high quality factors [3] and scalability for multi-analyte sensing using arrays of sensor elements [4, 5]. An important figure-of-merit of the Silicon photonic sensor is its detection limit, or the smallest change of refractive index that can be reliably measured by the system. In the past, highly sensitive Silicon microring sensors capable of measuring index shifts with a detection limit close to 10^{-7} Refractive Index Units (RIU) have been reported [6]. An important factor that influences the detection limit of the Silicon microring sensor is the variation in operating temperature of the device. This has several causes such as fluctuations in the ambient temperature, differences in the temperatures of sensor chip and the external analyte reservoir and local heating caused by viscous dissipation [7]. Owing to the high thermo-optic coefficient (TOC) of Silicon ($1.86 \times 10^{-4}/\,^{\circ}\mathrm{C}$) [8], small temperature fluctuations of the device can cause significant but undesirable shifts of resonances in a microring sensor [9]. Usually, closed loop controller platforms using Peltier Thermo-Electric Coolers (TECs) are employed to compensate random temperature fluctuations. However, it is difficult to track and correct localized thermal variations on the chip surface using external temperature controllers in real-time with sufficient accuracy. This is due to the considerably large response time of closed loop controllers, which typically ranges from a few seconds to above a minute depending on the thermal mass of the sensor system. More importantly, the Silicon carrier and buried oxide layers in an SOI wafer present a barrier for real-time measurement of surface temperature variations using a bottom-of-the-chip temperature sensor. In the past, reference microring resonators have been employed to compensate for measurement errors caused by temperature fluctuations on the sensor surface [10, 11]. In this approach, resonance shifts caused by temperature variations are tracked using a dedicated reference microring unexposed to the analyte being probed. Subtraction of resonance shift of reference microring from that of the sensor ring gives the required signal shift caused by a change in refractive index of analyte. However, this method suffers from a few drawbacks. Firstly, imperfections in fabrication processes can result in differences between dimensions of waveguides forming reference and sensor microrings,

Optics EXPRESS

causing an imbalance in the spectral responses to temperature shifts. Furthermore, the spatial separation between the reference and sensor microrings can result in differences of temperature variation profiles resulting in imperfect compensation of errors in wavelength shifts. To overcome these drawbacks, we propose and demonstrate the use of analyte TOCs for compensating errors in RI measurements caused by variations in ambient temperature. TOCs of analyte liquids are extracted from measurements of resonance wavelength shifts induced by controlled increments in the chip temperature. Metal rings patterned around Silicon microrings are used to monitor fluctuations of ambient temperature through measurement of variations in electrical resistance. Using this method, thermo-optic coefficients of three standard liquids; De-ionized water, Ethanol and Isopropanol were measured and are shown to be in good agreement with literature reports. Specifically, the TOC of De-ionized water was measured as $-1.12 \times 10^{-4}/\,^{\circ}\mathrm{C}$ with estimated error limits of $\pm 8.26 \times 10^{-6}/\,^{\circ}\mathrm{C}$. Chip surface temperature tracking is demonstrated with an instrument limited accuracy of 0.004 °C. Furthermore, we recorded a 16 factor enhancement in temperature tracking accuracy in comparison to global-scale monitoring. It is shown that the refractive index measurement precision of the microring is also improved by the same factor. We also discuss sensing schemes that eliminate the requirement of TEC based temperature controllers for RI shift measurements in specific cases where TOCs of analytes are known beforehand as standard values.

2. Theory

Resonance shifts observed in a microring sensor can be expressed as the sum of two components; the first caused by variation in analyte index and the second by fluctuations in ambient temperature. That is,

$$\Delta\lambda_{obs} = \Delta\lambda_{sen} + \left(\frac{\delta\lambda}{\delta T}\right)_{cl} \cdot \Delta T \tag{1}$$

Here, $\Delta\lambda_{sen}$ is the shift in resonance caused by variation in analyte index, $\left(\frac{\delta\lambda}{\delta T}\right)_{cl}$ is the rate of resonance wavelength shift with cladding liquid index change and ΔT denotes fluctuations in ambient temperature. We note that Eq. (1) can directly be used to extract the wavelength shift component $\Delta\lambda_{sen}$. However, it is advantageous to express the second term on right hand side of Eq. (1) in terms of thermo-optic coefficients since this may be known beforehand for standard analytes. If the TOC an analyte is not known, it can be extracted through measurements of wavelength shift rate $\left(\frac{\delta\lambda}{\delta T}\right)_{cl}$. Any variation in the temperature of microring causes shifts in the refractive indices of the waveguide core, buried oxide and the cladding liquid. In turn, this causes a net change in the effective index of the microring waveguide. Using the theory developed for athermal operation of Silicon photonic devices [12], one can express the net effective index change per unit variation in temperature as,

$$\frac{\delta n_{eff}}{\delta T} = \Gamma_{co}\frac{\partial n_{co}}{\partial T} + \Gamma_{box}\frac{\partial n_{box}}{\partial T} + \Gamma_{cl}\frac{\partial n_{cl}}{\partial T} \tag{2}$$

Here, Γ_i is the confinement factor in core, buried oxide or the upper/side cladding while $\frac{dn_i}{dT}$ are the thermo-optic coefficients. The confinement factor Γ is defined as [13],

$$\Gamma_s = \frac{n_g}{n_s}\left(\frac{\iint_s \epsilon|E|^2\,\mathrm{dxdy}}{\iint_{tot} \epsilon|E|^2\,\mathrm{dxdy}}\right) = \frac{n_g}{n_s}\gamma_s \tag{3}$$

In this expression, n_s is the refractive index of the waveguide constituent (core/cladding/oxide) under consideration. In the numerator, integration is performed over the cross section of the constituent 's'. Integral in the denominator covers the waveguide cross section entirely. γ_s is the fraction of power propagating within the region 's' and is termed as the 'fill factor'. Presence

Optics EXPRESS

of group index n_g in Eq. (3) indicates that confinement factors depend on the group velocity of propagating mode. To determine the TOC of analyte cladding $\left(\frac{\partial n_{cl}}{\partial T}\right)$, we rewrite the Eq. (2) as,

$$\frac{\partial n_{cl}}{\partial T} = \frac{\left(\frac{\delta n_{eff}}{\delta T}\right)_{cl} - \Gamma_{co}\frac{\partial n_{co}}{\partial T} - \Gamma_{box}\frac{\partial n_{box}}{\partial T}}{\Gamma_{cl}} \tag{4}$$

The rate of change of effective index $\left(\frac{\delta n_{eff}}{\delta T}\right)$ is obtained by measurement of resonant wavelength shifts $\left(\frac{d\lambda}{dT}\right)$, and substitution of results in the following expression:

$$\frac{\partial n_{eff}}{\partial T} = \frac{n_g}{\lambda_{res}}\frac{\Delta\lambda}{\Delta T} \tag{5}$$

where, λ_{res} is the resonance wavelength. Furthermore, the TOC of Silicon $\left(\frac{\partial n_{co}}{\partial T}\right)$ is determined by performing resonance shift measurements with air cladded microrings and compared with values reported in literature. It can be obtained using the following equation:

$$\frac{\partial n_{si}}{\partial T} = \frac{\left(\frac{\partial n_{eff}}{\partial T}\right)_{air} - \Gamma_{box}\frac{\partial n_{box}}{\partial T}}{\Gamma_{co}} \tag{6}$$

In this case, the thermo-optic coefficient of air is neglected since the refractive index of air is relatively invariant to temperature variations [14]. Furthermore, in both Eqs. (6) and (4), the TOC of buried oxide $\left(\frac{\partial n_{box}}{\partial T}\right)$ is taken as $8.57 \times 10^{-6}/\,^{\circ}\mathrm{C}$ from literature reports [15]. Confinement factors Γ_i are computed by determining fill factors γ_i using modal simulations since we have accurate knowledge of the dimensions and refractive indices of core and the claddings.

Once the TOC is determined accurately, we can express Eq. (1) as,

$$\Delta\lambda_{obs} = \Delta\lambda_{sen} + \frac{\lambda_{res}}{n_g}\left(\Gamma_{co}\left(\frac{\delta n_{co}}{\delta T}\right) + \Gamma_{ox}\left(\frac{\delta n_{ox}}{\delta T}\right) + \Gamma_{cl}\left(\frac{\delta n_{cl}}{\delta T}\right)\right)\Delta T \tag{7}$$

We further approximate this equation in terms of wavelength shift rate $\left(\frac{\delta\lambda}{\delta T}\right)_{air}$ and TOC of analyte as,

$$\Delta\lambda_{obs} \approx \Delta\lambda_{sen} + \left(\left(\frac{\Delta\lambda}{\Delta T}\right)_{air} + \frac{\lambda_{res}}{n_g}\Gamma_{cl}\left(\frac{\delta n_{cl}}{\delta T}\right)\right)\Delta T \tag{8}$$

This approximation is valid since we show later that the fill factors of core, oxide and the cladding regions do not change significantly for air and liquid coverings. We can thus express the sensing component of resonance shift as,

$$\Delta\lambda_{sen} = \Delta\lambda_{obs} - \left(K_1 + K_2 \cdot \left(\frac{\delta n_{cl}}{\delta T}\right)\right)\Delta T \tag{9}$$

The constant $K_1 = \left(\frac{\Delta\lambda}{\Delta T}\right)_{air}$ can be measured as an initial calibration and used subsequently for correction of wavelength shifts. The second constant $K_2 = \frac{\lambda_{res}}{n_g}\Gamma_{cl}$ can be determined through simulations (for Γ) and spectrum measurements (for λ_{res} and n_g). Using the corrected wavelength shift $\Delta\lambda_{sen}$ and the resonance shift rate $\left(\frac{\Delta\lambda}{\Delta n_{cl}}\right)$, the expected refractive index shift of analyte can now be obtained using the expression,

$$\Delta n_{cl} = \frac{\Delta\lambda_{sen}}{\left(\frac{\Delta\lambda}{\Delta n_{cl}}\right)} \tag{10}$$

Optics EXPRESS

3. Design of TOC measurement system

Schematic of the system used for wavelength shift measurements is shown in Fig. 1(a). The photonic chip consists of several identical Silicon microring resonators for redundancy. Metal rings are patterned concentrically around each resonator, at a distance of about 2μm, for measurement of temperature variations. Low resistance Gold contact lines are defined for electrical probing of metal rings. A PDMS (Polydimethylsiloxane) reservoir structure provides containment for liquid analyte. The chip is placed on a temperature controlled platform consisting of a peltier heater powered by a temperature controller instrument. A copper base plate is mounted on the peltier element for equalization of temperature and efficient transfer of heat to the sensor chip. A Resistance Temperature Detector (RTD) element attached to the copper base plate was interfaced to the controller for closed-loop tracking of chip temperature. Waveguides and microrings were implemented using photonic wires (400 nm$\times$ 220 nm) operating with fundamental TE-like mode at 1550 nm wavelength band. Since the core material Silicon has a linear expansion coefficient of $2.59\times10^{-6}/\,^{\circ}$C, change in waveguide dimensions over the relatively small operating temperature range (about 12 $^{\circ}$C) is not considered in our analysis. We used finite element method modal

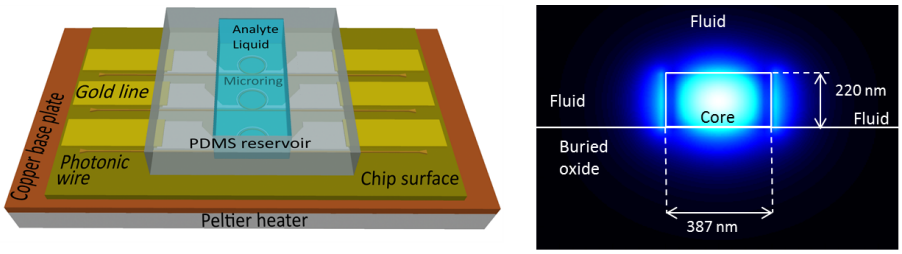

Fig. 1. Design and simulation of Silicon microring TOC sensor (a) A schematic showing the photonic sensor chip. (b) Simulation result showing the distribution of electric field (TE-like mode) along the cross section of a photonic wire waveguide.

analysis software for computing fill factors. Figure. 1(b) shows the field distribution across the photonic wire. Width and height of the simulated waveguide structure were set to 387 nm and 220 nm respectively after analyzing the scanning electron microscope (SEM) images of the fabricated device. Thickness of the buried oxide layer was set to 2 μm, based on wafer specifications. Refractive index of tested analyte liquids (at 1550 nm), forming the upper and side clads were taken from literature [16]. Tab. 1 shows the simulated fill factors for air and analyte claddings. For comparison, we have also measured the refractive index of the analytes at 590 nm wavelength using a commercial Abbe refractometer, as shown in the table.

Table 1. **Simulation of confinement factors for different claddings of the photonic wire (387 nm $\times$ 220 nm) at working wavelength of 1510 nm.**

Fluid	Ref. Index (1550 nm)	Ref. Index (590 nm)	γ_{co}	γ_{cl}	γ_{box}	n_{eff}	n_g
Air	1	1	0.727	0.113	0.146	2.129	4.64
DI Water	1.3164 [16]	1.333	0.71	0.142	0.132	2.208	4.37
Ethanol	1.3503 [16]	1.359	0.708	0.145	0.13	2.217	4.34
Isopropanol	1.3661 [16]	1.373	0.707	0.147	0.129	2.221	4.33

Optics EXPRESS

4. Experiments and results

4.1. Device fabrication and experimental methods

An SOI wafer with 220 nm thick device layer and 2μm buried oxide was used for fabrication of the sensor chip. In the first step, Electron beam (e-beam) lithography was performed using a negative tone resist (ma-N2401) for definition of photonic wires, microrings and bases for grating couplers. The radius of microrings was designed to be 100 μm, and the width of metal ring was set to 2 μm. A dry etch step using fluorine chemistry was used to transfer resist patterns to the SOI device layer. Following this, a second E-beam lithography process was carried out using a positive tone (PMMA) resist coating for patterning gratings over previously formed bases. These patterns were transfered onto SOI layer using dry etch. A third step of e-beam exposure process (with PMMA resist) was employed for definition of metal ring patterns. This was followed by sputtering of metal bi-layer (Titanium-10 nm/ Platinum 50 nm) and lift-off processes to obtain metal structures. Subsequently, optical lithography and metal lift off (Chromium-10 nm/ Gold-90 nm) steps were used for definition of low resistance contact strips for electrical probing. A positive tone resist (S1813) was used for this process. Finally, a containment structure prepared using PDMS was bonded over the sensor chip to serve as a reservoir for analyte liquid over microrings. Figure. 2 shows images of patterns at various stages of fabrication.

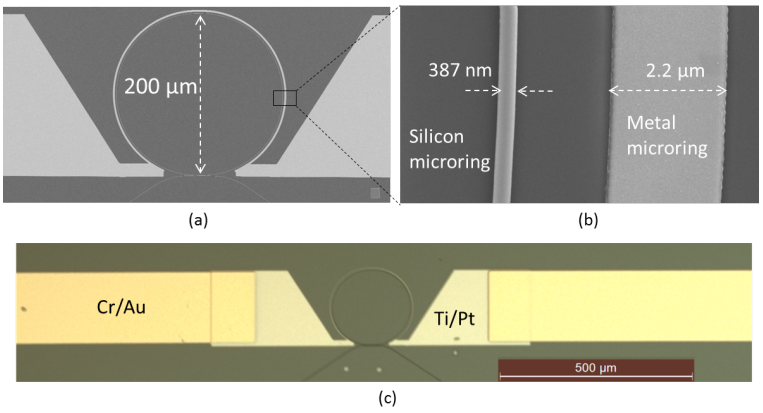

Fig. 2. Images of fabricated microrings and metal rings for thermo-optic coefficient measurement. (a) Scanning Electron Microscope (SEM) image of Silicon microring surrounded by platinum metal ring (b) Magnified view of the wire waveguide and metal ring (c) Microscope image showing gold contact lines for electrical probing of metal rings

An optical source-detection module consisting of a tunable Laser (1505-1620 nm), and an InGaAs power meter was used for spectral measurements. Grating couplers fabricated on chip were used to couple light in and out of the photonic sensor chip through a single mode (SMF-28) optical fibre. A high precision source-measurement unit was used to monitor the electrical resistance of metal rings and thereby track the on-chip temperature variations.

4.2. Calibration of resistive metal rings

The on-chip resistive metal ring was first calibrated using a device probe station equipped with a high precision thermal chuck and a semiconductor device analyzer. This experiment was performed with air cladded microrings and hence the PDMS reservoir was not filled with any liquid. Electrical resistance of the metal ring was monitored for increasing temperatures of the chuck. From the resistance-temperature plot, we extracted the slope of resistance variation to

Optics EXPRESS

be 2.45 Ω/ °C, as shown in Fig. 3(a) as the reference plot. Subsequently, we used the assembly described in Sec. 2 to perform resistance slope measurements. In this case, the closed-loop temperature controller was used to heat the photonic chip to the desired temperature. As mentioned earlier, a source measurement unit (SMU) was used to monitor the electrical resistance of the metal ring. In this case, the mean slope (3 trials) of resistance variation with temperature was measured to be 2.46 Ω/ °C, as shown in Fig. 3(a). This experiment was repeated after filling the PDMS reservoir with DI-water to understand the effect of thermal mass of liquids on chip surface temperature variation. We ensured that the voltage applied to metal rings for resistance measurement was kept below the electrolytic potential of water (1.23V) to avoid electrolysis. The measured slope of resistance variation (mean value) in this case was 2.48 Ω/ °C, as seen in Fig. 3(b). Evidently, the thermal mass of a small volume of water (few microliters) does not cause significant difference in the temperature variation in comparison to that with air covering the device.

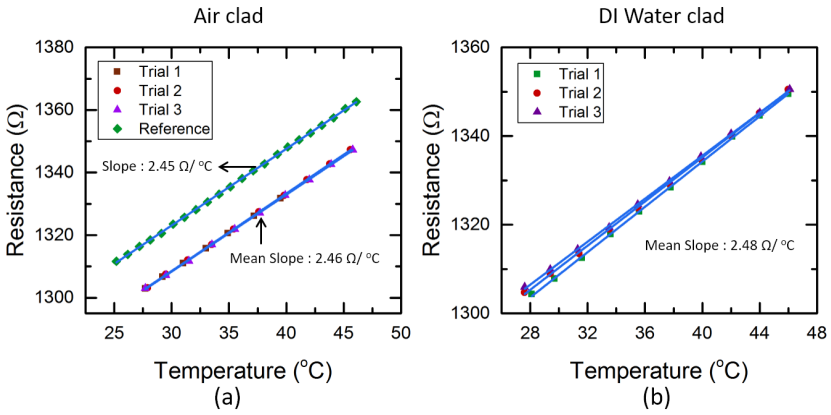

Fig. 3. Measurements of metal ring resistance versus temperature (a) With air covered microrings. The reference data was obtained using a calibrated thermal chuck. Three trials were performed using our characterization assembly (b) With DI-water covered microrings. The R^2 value exceeded 0.99 for all linear fits.

4.3. *Measurement of thermo-optic coefficients*

The theory described in the previous section was first used to determine the TOC of Silicon. A good agreement of our measurements with literature reports would validate the described TOC measurement method. The PDMS reservoir was left unfilled so that air forms the upper and side claddings of the waveguide. Temperature of the photonic chip was varied using the closed loop controller while resonant wavelength shifts were monitored. Measured full width half maximum (FWHM) of resonances was about 0.1 nm, with an FSR of 0.79 nm. A linear fit was used to express the wavelength shift as a function of the chip temperature [Fig. 4(a)]. Mean slope $\left(\frac{\Delta\lambda}{\Delta T}\right)_{air}$ of three trials was calculated to be 62.72 $pm/\,^{\circ}$C [Fig. 4(b)]. Upon substitution of relevant parameters in Eq. (6) the TOC of Silicon was calculated as $1.92 \times 10^{-4}/\,^{\circ}$C. While this value is about 3.2% higher than the commonly reported Silicon TOC of $1.86 \times 10^{-4}/\,^{\circ}$C, we note that the TOC itself is a function of temperature. Specifically, Frey. *et. al.* [8] have tabulated TOC values of Silicon for different temperatures and a range of wavelengths. Based on this reference, we computed the value of Silicon TOC at a mean temperature of 35 °C to be $1.93 \times 10^{-4}/\,^{\circ}$C, which differs by about 0.5% from our measurement.

Optics EXPRESS

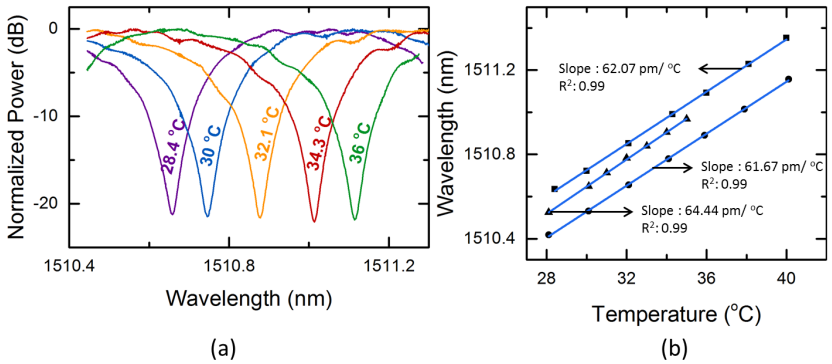

Fig. 4. Measurements for determination of TOC: Silicon (a) Positions of a transmission resonance for different temperatures. (b) Shift in resonance position as a function of temperature (3 trials). R^2 value for all curve fits exceeded 0.99.

For experiments with De-ionized water, the PDMS reservoir was filled with a small quantity of the liquid using syringes. Wavelength shift measurements were performed as described before. The TOC was calculated by substituting wavelength shift slopes $\left(\frac{\Delta\lambda}{\Delta T}\right)_{cl}$ and the simulated parameters of Tab. 1 in Eq. (4). The mean slope (3 trials) of resonance wavelength shift is 42.95 $pm/\,^{\circ}\mathrm{C}$ [Fig. 5]. The decreased slope of wavelength shift relative to that of air clad is a result of reduction in the rate of change of effective index shift $\left(\frac{\partial n_{eff}}{\partial T}\right)$ owing to the negative thermo-optic coefficient of water. Using Eq. (4) and simulated parameters of Tab. 1 we calculated the TOC of DI-Water to be $-1.12 \times 10^{-4}/\,^{\circ}\mathrm{C}$. This value compares well with those reported previously in literature, as shown in Tab. 2.

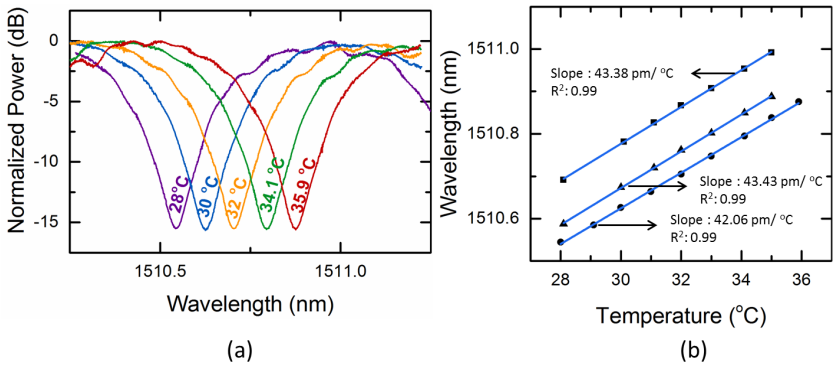

Fig. 5. Measurements for determination of TOC: De-ionized water (a) Positions of a transmission resonance for different temperatures. FWHM of resonances is about 0.3 nm. relative to that of air cladding (b) Shift in resonance position as a function of temperature. R^2 value for all curve fits exceeded 0.99.

Next, we measured the TOCs of organic solvents Ethanol and Isopropanol. Optical constants of these liquids have been well documented in literature. We limited the experiments with solvents to a maximum of two trials to avoid disintegration of PDMS reservoir due to swelling [17]. Between measurements involving different liquids, the chip was cleaned using DI water, dried

Optics EXPRESS

with nitrogen flow and heated to remove trace moisture. For Ethanol [Fig. 6(a)], we see that the wavelength shift slope is reduced further to 18.95 $pm/\,^{\circ}$C, owing to stronger negative TOC which is calculated to be $-2.59 \times 10^{-4}/\,^{\circ}$C. In case of Isopropanol, the mean wavelength shift slope (of two trials) is negative at -7.99 $pm/\,^{\circ}$C. That is, the effective index shift rate $\left(\frac{\partial n_{eff}}{\partial T}\right)$ of Eq. (5) is negative indicating that the effect of TOC of cladding liquid outweighs that of core Silicon, as seen in Fig. 6(b). Upon substitution of relevant parameters in Eq. (4), we obtain the TOC of Isopropanol to be $-4.25 \times 10^{-4}/\,^{\circ}$C.

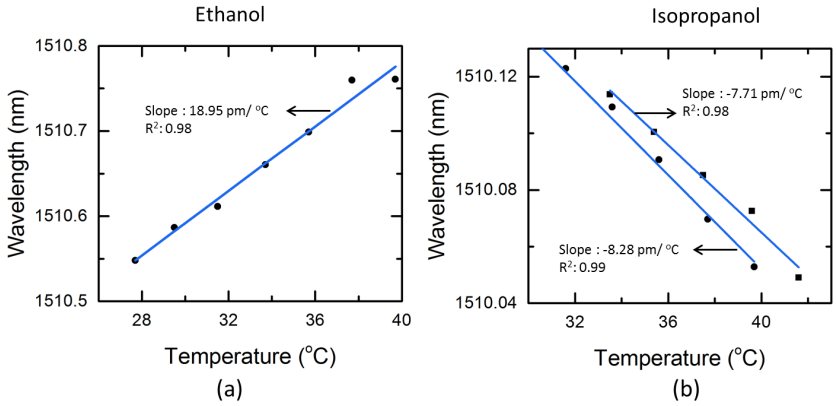

Fig. 6. Measurements for determination of TOC: Organic liquids (a) Resonance wavelength shifts for ethanol cladding. (b) Shifts in resonance wavelength for IPA cladding. In this case, the slope is negative owing to very strong (negative) TOC of the analyte.

Thermo-optic coefficients measured using the described method are largely in good agreement with literature reports, as seen in Tab. 2, although a slight deviation is observed in case of Ethanol. As mentioned before, we could not perform multiple measurement trials with organic solvents owing to the possibility of damage to the PDMS structure. Better convergence with literature reports is expected with more measurement iterations using a compatible reservoir material.

Table 2. **Comparison of thermo-optic coefficients determined by our study with values reported in literature near 1550 nm wavelength band.**

Fluid	Our study	Literature Reports	References
DI Water	$-1.12 \times 10^{-4}/\,^{\circ}$C	$-7.65 \times 10^{-5}/\,^{\circ}$C, $-1.241 \times 10^{-4}/\,^{\circ}$C	[18], [19]
Ethanol	$-2.59 \times 10^{-4}/\,^{\circ}$C	$-3.69 \times 10^{-4}/\,^{\circ}$C, $-3.38 \times 10^{-4}/\,^{\circ}$C	[18], [19]
Isopropanol	$-4.25 \times 10^{-4}/\,^{\circ}$C	$-4.5 \times 10^{-4}/\,^{\circ}$C, $-4 \times 10^{-4}/\,^{\circ}$C	[20], [21]

4.4. Calculation of error limits for TOC measurements

It is important to determine the influence of uncertainties in various simulated and measured parameters on the calculations of thermo-optic coefficient. We analyzed the effect of variation of several critical parameters in Eq. (4) and their effect on the TOCs of fluids. Major contributions towards uncertainties in TOC calculations arise from discrepancies in the wavelength shift slope measurements and variations in the width of waveguides used for fill factor simulations. Other sources of deviations in TOC calculations include uncertainty in the absolute refractive index of

Optics EXPRESS

liquids used in simulations, and variations in field confinement factors over the measurement temperature range. However, our calculations showed that the latter two sources are at least an order of magnitude lower than the first two in terms of contribution towards variations in measurements, and were therefore not analyzed further.

Random variations in slopes of resonance wavelength shifts are a result of various noise affecting the measurement system. To obtain an estimate of this variation, we performed seven iterations of slope measurements for the DI-water analyte using the procedure described earlier. Results of these measurements are plotted in Fig. 7. The coefficient of determination (R^2 value) for curve fits was greater than 0.99 in all trials indicating good linearity of wavelength shifts and also the quality of estimated slopes. Standard deviation ($\sigma_{\Delta\lambda/\Delta T}$) of seven wavelength shift slopes values was calculated to be 1.044 $pm/\,^{\circ}\mathrm{C}$. The mean value of slope measured in this set of trials (37.96 $pm/\,^{\circ}\mathrm{C}$) differs slightly from that shown in Fig. 5(b) due to some differences in calibration of the closed loop temperature controller system.

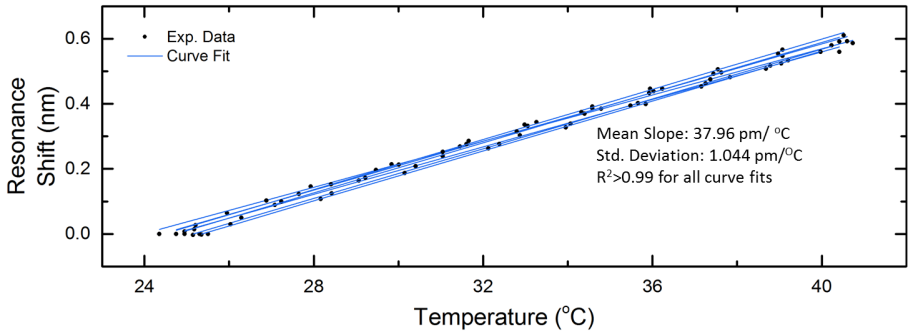

Fig. 7. Determination of error limits of TOC of water. Seven iterations of wavelength shift slope measurements were performed.

Upon substitution of Eq. (5) in Eq. (4) and subsequent differentiation of the equation with respect to the slope $\frac{\Delta\lambda}{\Delta T}$ we obtain the following expression.

$$e_{\Delta\lambda/\Delta T} = \frac{n_{cl}}{\gamma_{cl}} \frac{\sigma_{\Delta\lambda/\Delta T}}{\lambda_{res}} \tag{11}$$

This equation translates variations in slope measurements ($\sigma_{\Delta\lambda/\Delta T}$) into equivalent uncertainty in TOC estimations which is calculated to be $e_{\Delta\lambda/\Delta T} = 6.42 \times 10^{-6}/\,^{\circ}\mathrm{C}$.

Next, we determined the effect of variations in width of waveguide cores on the estimates of TOC. Through measurements on SEM images taken at different positions on the microring, we computed the mean and standard deviation (σ_w) of widths to be respectively 387 nm and 4.5 nm. Upon differentiation of Eq. (4) with respect to width of waveguide core, we obtain the following expression:

$$e_w = \left| \frac{n_{cl}}{\gamma_{cl}} \left(\frac{1}{\lambda_{res}} \frac{\Delta\lambda}{\Delta T} - \frac{1}{n_{co}} \left(\frac{\partial n_{si}}{\partial T} \right) \frac{\partial \gamma_{co}}{\partial w} \right) - \left(\frac{n_{cl}}{\gamma_{cl}^2} \frac{\partial \gamma_{cl}}{\partial w} \right) \left(\frac{1}{\lambda_{res}} \frac{\Delta\lambda}{\Delta T} - \frac{\gamma_{co}}{n_{co}} \frac{\partial n_{si}}{\partial T} \right) \right| \sigma_w \tag{12}$$

Here, $\frac{\partial \gamma_{co}}{\partial w}$ and $\frac{\partial \gamma_{cl}}{\partial w}$ are the rates of change of field fill factors in the core and analyte fluid clads with respect to change in width (w) of the core. In deriving Eq. (12), we have not considered the effect of variation in the buried-oxide fill factor since the contribution of the term is more than an order of magnitude lower than those due to variations in γ_{cl} and γ_{co}. Using modal simulations with waveguide core as the variable we found the derivatives of fill factors as

Optics EXPRESS

$\frac{\partial \gamma_{c0}}{\partial w} = 1.09/\mu m$ and $\frac{\partial \gamma_{c1}}{\partial w} = -0.625/\mu m$. Substituting these results in Eq. (12) we obtain the contribution towards uncertainty in TOC to be $e_w = 5.19 \times 10^{-6}/\,^{\circ}\mathrm{C}$. The combined effect deviations introduced by slope shift uncertainty $e_{\Delta\lambda/\Delta T}$ and core width variations e_w is obtained by computing the square root of squares of individual contributions. This value is computed to be $e_{TOC-DIW} = 8.26 \times 10^{-6}/\,^{\circ}\mathrm{C}$ which is about 7 % of the calculated TOC of DI water. If the device is used for measurement of variations in TOC due to changes in physical/chemical properties of liquids, the detection limit of TOC is desired. This is taken as three times the standard uncertainty, which for our system computes to be $2.47 \times 10^{-5}/\,^{\circ}\mathrm{C}$.

4.5. On-chip temperature tracking using metal rings

Lastly, we performed experiments to demonstrate the precision temperature tracking capability using the metal rings. Ambient thermal fluctuations cause shifts in the optical resonances of microrings as well as variations in the electrical resistance of metal rings. The extent of temporal correlation between these signals depends on their spatial separation. For these measurements, the controller was set to maintain a fixed temperature at the copper base plate. Resonant wavelength shifts and electrical resistance variations were monitored simultaneously over a few minutes, with a sampling interval of about 5 seconds [Fig. 8]. For resistance measurements, three consecutive

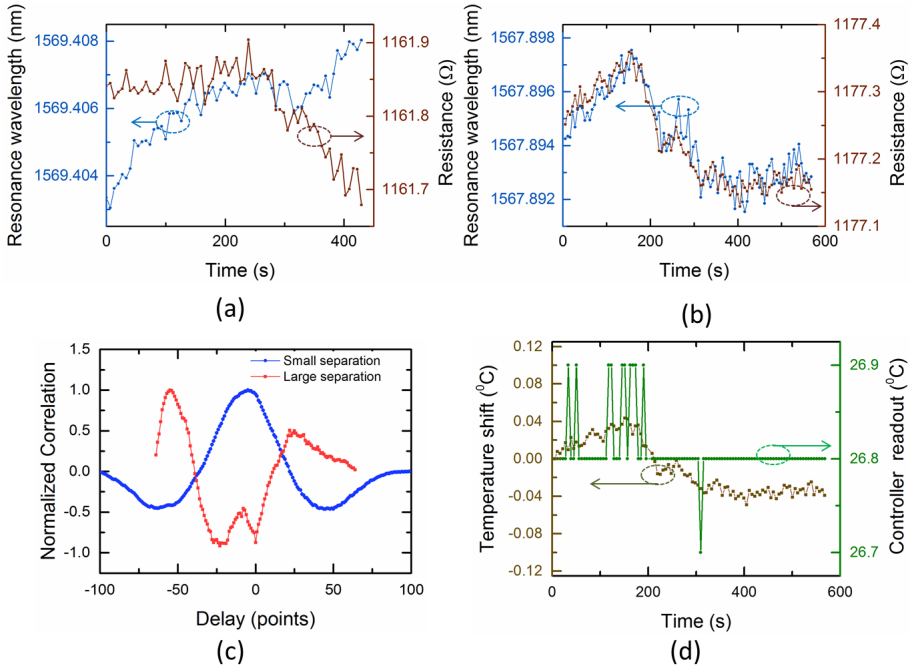

Fig. 8. Measurement of ambient thermal fluctuations. (a) Wavelength shift and resistance measurements on Silicon microring and a metal ring spaced apart by about 500 μm (centre to centre), showing uncorrelated variations of quantities. (b) Measurements for concentric microring and metal ring as shown in Fig. 2(b). (c) Cross-correlation plots of wavelength shift and resistance variation signals. A good correlation is observed between the signals for small separation between microring and metal ring at zero delay position. In contrast, no clear trend is visible in the correlation output for large separation between metal and silicon rings. (d) Temperature variation as calculated by resistance measurement, compared with the read-out of the temperature controller.

Optics EXPRESS

values (acquired within about 0.3 seconds) were averaged to obtain a single data point for noise reduction. Curve fitting was used for tracking wavelength resonance minimum precisely. These experiments were performed with air as the upper and side claddings. However, we note that the method can be implemented for liquid analyte claddings as well. To understand the effect of spatial separation on the resonance and resistance shift signals, we first measured the wavelength shift in one microring while monitoring electrical resistance of a metal ring whose centre was about 500 μm away from that of the microring. Results of this experiment are shown in Fig. 8(a). We see different profiles of wavelength shifts and resistance variations, indicating that relatively small spacing of a few hundred micrometers results in de-correlation of local temperature fluctuations. In the second experiment, another device having the metal ring concentrically patterned around the Silicon microring as shown in Fig. 2(b) was used. As seen in the figure, spacing between the metal strip and Silicon waveguide is about 2 μm. In this case, a very good correlation between resistance variation and resonance shifts is observed in the plots shown in Fig. 8(b), proving that the temperature tracking must be performed in close proximity of the sensing microring for best results. This is also clear from the correlation plots shown in Fig. 8(c). Using the resistance variation coefficient of 2.48 $\Omega/\,^{\circ}$C determined previously, we plot the fluctuation of ambient temperature in Fig. 8(d). The measurement precision of resistance depends on the noise performance of electrical equipment, which in this case is a source measurement unit (Keithley 2400). Based on the instrument specifications, the noise levels at the probing voltage (1V) and current (0.83 mA) levels were taken as 10 μV and 10 nA. From these values, we estimated the uncertainty in resistance calculations to be 0.0109 Ω, after accounting for noise reduction achieved by averaging three samples. This results in a temperature measurement accuracy of 0.004 $^{\circ}$C using the resistance variation coefficient of 2.48 $\Omega/\,^{\circ}$C.

An important comparison between the accuracies of temperature measurement at the surface and bottom of the chip be drawn by analyzing data plotted in Fig. 3. By performing residual analysis on the reference plot of Fig. 3(a), we obtained the standard deviation of differences between the chuck and on-surface temperatures as 0.072 $^{\circ}$C. Therefore, by monitoring the temperature variation on-chip near the sensor microring, we obtain a tracking accuracy enhancement by a factor of 16.39. Equation. (9) may be used to understand how this enhancement translates to improved detection limits of refractive index. When the refractive index of the analyte liquid is unaltered, the sensing component of wavelength shift (λ_{sen}) must be zero. Any resonance shift observed (λ_{obs}) is now due to fluctuations in ambient temperature. Owing to more accurate compensation of temperature induced shifts, the uncertainty in resonance shifts is reduced by a factor of 16.39 using on-chip temperature tracking in our system. In effect the refractive index detection limit is improved by the same factor in accordance with Eq. (10), assuming the optical readout equipment can measure resonance shifts with sufficient precision. More importantly, if the TOC of analyte is known beforehand, and the wavelength shift rate with air cladding $\left(\frac{\Delta\lambda}{\Delta T}\right)_{air}$ is specified for the chip at manufacture, the necessity of a closed loop temperature control is obviated, enabling considerable reduction in system complexity and operational costs.

5. Conclusion

We have reported a method for compensation of errors caused by temperature variations in Silicon microring sensors. Specifically, the thermo-optic coefficient is used for in conjunction with real-time, on-chip temperature monitoring to compensate for deviations in measured wavelength shifts. Using the field confinement theory in high contrast waveguides, we have formulated an expression for describing the thermo-optic coefficient of a liquid in terms of field confinement factors. Variations in temperature near the microring is tracked by monitoring electrical resistance of a metal ring structure. Experiments for measurement of thermo-optic coefficients of Silicon and analyte liquids are described. TOC values determined through our experiments are in good

Optics EXPRESS

agreement with literature reports. We have also discussed possible errors in TOC calculations resulting from uncertainties of various parameters. In our experiments, we could demonstrate an improvement in temperature tracking accuracy by a factor of 16, limited only by noise in electrical probing instruments. A dedicated low noise electronic circuit can potentially provide better resistance measurement precision, enabling further improvements in error compensation of refractive index shift measurements. Furthermore, we have used an external peltier heater linked to a closed loop temperature controller for heating the chip during TOC measurements. As an alternative, the metal ring used for temperature monitoring can itself possibly be used to heat the analyte while simultaneously tracking variation in resistance to deduce temperature increments. We were not successful in achieving this due to electrolysis of polar liquids, once the applied voltage to the metal ring exceeded the electrolytic potential. To circumvent this problem, a thin layer of insulating di-electric can be coated to electrically isolate the metal ring from the analyte liquid. With the improvements suggested here, one can realize a compact, high performance refractive index and thermo-optic coefficient sensor that can achieve better detection limits than device configurations reported previously in literature.

Acknowledgments

Authors thank the staff of National Nano-Fabrication Centre (NNFC), and Micro and Nano Characterization Facility (MNCF) at the Indian Institute of Science-Bangalore, for their assistance. PRP is grateful to the Ministry of Human Resource Development, Government of India for funding his scholarship. SKS thanks the Ministry of Electronics and Information Technology, Government of India for support.

Disclosures

The authors declare that there are no conflicts of interest related to this article.